www.czasopisma.pan.pl PAN POLSKA AKADEMIA NAUK www.journals.pan.pl

Metrol. Meas. Syst., Vol. 23 (2016), No. 3, pp. 383–391.

PAN POLSKA AKADEMIA NAUK

METROLOGY AND MEASUREMENT SYSTEMS

Index 330930, ISSN 0860-8229

www.metrology.pg.gda.pl

M&MS

ESTIMATION OF FLIGHT PATH DEVIATIONS FOR SAR RADAR INSTALLED ON UAV

Michał Łabowski, Piotr Kaniewski, Stanisław Konatowski

Military University of Technology, Faculty of Electronics, Kaliskiego 2, 00-908 Warsaw, Poland
(✉ mlabowski@wat.edu.pl, +261 837 469, *pkaniewski@wat.edu.pl, skonatowski@wat.edu.pl)*

Abstract

The paper presents a method of calculation of position deviations from a theoretical, nominally rectilinear trajectory for a SAR imaging system installed on board of UAV. The UAV on-board system consists of a radar sensor, an antenna system, a SAR processor and a navigation system. The main task of the navigation part is to determine the vector of differences between the theoretical and the measured trajectories of UAV center of gravity. The paper includes chosen results of experiments obtained during ground and flight tests.

Keywords: Unmanned Aerial Vehicle, Synthetic Aperture Radar, Inertial Measurement Unit, Global Navigation Satellite System.

1. Introduction

For simplicity of radar imaging algorithms an *Unmanned Aerial Vehicle* (UAV) with an on-board SAR (*Synthetic Aperture Radar*) system should move with a constant velocity and follow a straight flight path. In the case of a mini-UAV, due to its small size, weight and velocity, maintaining the rectilinear trajectory, in the unstable atmosphere, is not possible [1]. Therefore, compensation techniques, which modify the phase of the echo signal, are frequently applied. In many solutions a navigation system is used to determine the position of UAV in relation to the assumed, theoretical trajectory. Another possible option consists in calculation of position deviations based on effects observed in the echo signal. However, this paper focuses on the algorithms for determining navigation corrections based on the difference between the real and the theoretical trajectory of the UAV *Centre Of Gravity* (COG) using an on-board navigation system. The corrections estimated by the navigation system can then be used to determine the slant range between the UAV COG and the target which enables to calculate the proper phase of the echo signal. Uncorrected deviations from the assumed trajectory exceeding $0.1\,\lambda$ introduce significant phase errors and deteriorate the quality of SAR images [2]. In some authors' opinion the fully focused SAR imaging requires the positioning accuracy better than $0.25\,\lambda$ [3]. The carrier frequency of the radar sensor used in our experiments is equal to 2.91 GHz, therefore $\lambda = 0.1034$ m. The above mentioned requirement poses a great challenge for the navigation system. However, thanks to the integration of data from an IMU (*Inertial Measurement Unit*) and a GNSS receiver (*Global Navigation Satellite System*) with the RTK (*Real Time Kinematic*) option it is possible to achieve the required accuracy.

Two versions of calculation of the flight path deviations are described in this paper. The proposed algorithms can be used in real-time applications as well as in post-processing routines.

Article history: received on Dec. 11, 2015; accepted on Apr. 11, 2016; available online on Jul. 18, 2016; DOI: 10.1515/mms-2016-0034.

2. Navigation system

The main reasons of UAV displacements from the assumed rectilinear trajectory are instabilities of the atmosphere and manoeuvres of UAV caused by operation of its autopilot. These movements change the distance from the radar to the target which affects the phase of the echo signal. It is possible to distinguish three types of displacements in the direction x, perpendicular to the theoretical flight path axis y [4] (Fig. 1).

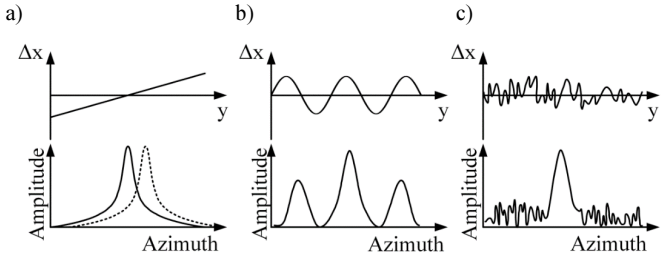

Fig. 1. The influence of movement instabilities on the single-point-target echo signal.

A constant velocity component along the x axis (Fig. 1a) shifts the center frequency of echo signal. In the case of sinusoidal-shaped displacements (Fig. 1b) additional high-level side lobes are observed. If the disturbances have a random character (Fig. 1c) the amplitude of noise is increased.

Besides the linear displacements from the rectilinear trajectory, the UAV can perform an unintended angular motion around its longitudinal, transversal and vertical axes. Among these elements the most significant can be non-zero, variable angle of sideslip (squint), caused by the wind. It leads to changes of the azimuthal position of radar footprint. In the case of a relatively short aperture synthesis period the influence of the squint effect on SAR images is minor, while the computational complexity of an algorithm trying to compensate this effect would be significantly increased. In real-time applications it is then possible to omit the effects caused by the orientation instabilities.

The navigation system is composed of a dual-antenna GNSS receiver with the RTK option and an accurate IMU. The GNSS and IMU data are processed together in a *Navigation Data Processing Module* (NDPM). The algorithms implemented in NDPM are: the *Strapdown Inertial Navigation System* algorithm [5, 6], the Kalman Filter [7–10] and the Navigation Correction algorithm. A method of calculation of position deviations uses several reference frames. The *b-frame* has its origin at the UAV COG, its x^b axis is aligned with its longitudinal axis, the y^b axis is directed towards the right wing, and the z^b axis completes the right-handed coordinate system [11]. The *l-frame* is a local horizontal frame with its origin at the UAV COG at the moment of start of a scanning session, the y^l axis coincides with the theoretical trajectory of flight and is related to the geographic North through an angle Ψ, the z^l axis points upwards. Thus, the theoretical course of flight Ψ is needed to establish the *l-frame* orientation. The ECEF (*Earth-Centred Earth-Fixed*) frame is a global frame with the coordinates: longitude λ, latitude φ and altitude h [11]. The NED frame is a local geographic frame with its axes aligned with the directions of North, East and local vertical [11].

The process of calculation of the position deviations consists in determining the position of the UAV COG in relation to the *l-frame*. It is assumed that the UAV moves only along the y^l axis, thus the position components along the x^l and z^l axes should be zero. Any non-zero value in these two axes can be interpreted as a trajectory deviation which should be passed as a message to the SAR processor. The components of this message are: the position errors along

Metrol. Meas. Syst., Vol. 23 (2016), No. 3, pp. 383–391.

the x^l and z^l axes as well as the position and velocity measured along the y^l axis. In the paper, two versions of the algorithm are presented. They differ in the location of the reference points used to determine the position deviations.

2.1. Navigation correction algorithm – version I

The position of the UAV COG at the beginning of a measurement session is interpreted as the origin of *l-frame*. It is assumed that UAV moves uniformly along the y^l axis and the course is constant. The theoretical course Ψ and the velocity along the y^l axis are received from the Ground Control Station at the beginning of the session. These parameters are used to calculate the points of theoretical positions of UAV COG during flight (for each packet of raw radar data). The NDPM calculates vectors of differences between the real (measured) and the reference (theoretical) positions of UAV (Fig. 2a), according to the formulae:

$$\begin{bmatrix} \Delta\varphi \\ \Delta\lambda \\ \Delta h \end{bmatrix} = \begin{bmatrix} \varphi \\ \lambda \\ h \end{bmatrix}_{real} - \begin{bmatrix} \varphi \\ \lambda \\ h \end{bmatrix}_{ref}, \tag{1}$$

where: $[\Delta\varphi \;\; \Delta\lambda \;\; \Delta h]^T$ – the vector of differences between the real and the reference (here: theoretical) position; $[\varphi \;\; \lambda \;\; h]^T_{ref\,/\,real}$ – the vector of reference/real position of UAV.

The position error is subsequently converted onto the NED reference frame. In this algorithm the origin of NED frame is the theoretical position of UAV COG calculated for the actual radar data (Fig. 2b):

$$\begin{bmatrix} \Delta N \\ \Delta E \\ \Delta D \end{bmatrix} = \begin{bmatrix} R_m + h_{ref} & 0 & 0 \\ 0 & (R_p + h_{ref})\cos\varphi_{real} & 0 \\ 0 & 0 & -1 \end{bmatrix} \begin{bmatrix} \Delta\varphi \\ \Delta\lambda \\ \Delta h \end{bmatrix}, \tag{2}$$

where: $[\Delta N \;\; \Delta E \;\; \Delta D]^T$ – the vector of differences between the reference and the real position of UAV expressed in NED; $R_{m\,/\,p}$ – the meridian/transverse radius of curvature.

Finally, the position error is converted onto the *l-frame* using:

$$\begin{bmatrix} \Delta x \\ \Delta y \\ \Delta z \end{bmatrix} = \begin{bmatrix} -\sin\Psi & \cos\Psi & 0 \\ \cos\Psi & \sin\Psi & 0 \\ 0 & 0 & -1 \end{bmatrix} \begin{bmatrix} \Delta N \\ \Delta E \\ \Delta D \end{bmatrix}, \tag{3}$$

where $[\Delta x \;\; \Delta y \;\; \Delta z]^T$ is the vector of differences between the theoretical and the real position of UAV expressed in the *l-frame*.

The real position and velocity measured along the y^l axis can be computed based on:

$$y^l_{real} = y^l_{ref} + \Delta y, \tag{4}$$

$$v_y = v_N \cos\Psi + v_E \sin\Psi, \tag{5}$$

where: $y^l_{real/ref}$ – the real/theoretical position along the y^l axis, v_y – the real velocity component measured along the y^l axis; $v_{N/E}$ – the North/East component of the real velocity vector of UAV.

The advantage of this algorithm is its method of determining the origin of NED frame. For a particular radar measurement it is located in the theoretical position of UAV COG. Given that

the altitude above ellipsoid for all theoretical points is constant, the NED frame displaces with the UAV, rotates and follows the curvature of Earth. This can be essential for sessions in which UAV travels significant distances. However, this method requires knowledge of the theoretical course and velocity at the beginning of a measurement session. This may be considered as a drawback, since assuming an invalid value of velocity affects correctness of theoretical position estimation.

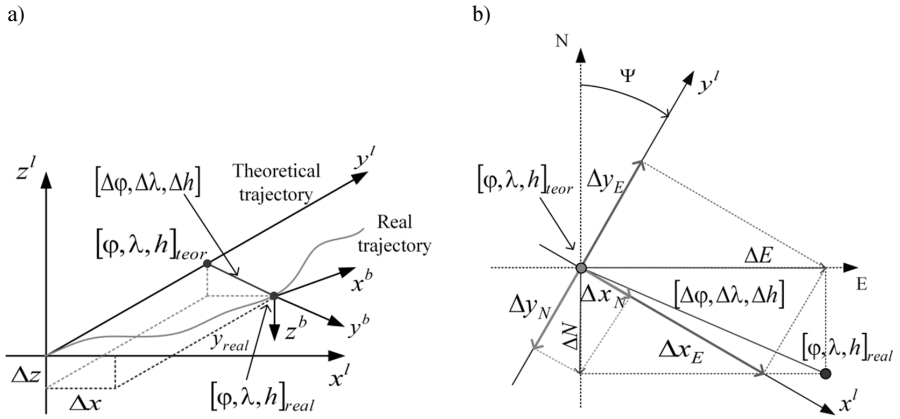

Fig. 2. Computation of the position error: a) in ECEF frame; b) in NED and l-frame.

2.2. Navigation correction algorithm – version II

In the version II of algorithm, the theoretical positions of UAV COG are not calculated for each radar measurement, and there is only a single reference point, which is the origin of *l-frame* (Fig. 3). Thus, there is no need to know the theoretical velocity of UAV along the y^l axis, only the theoretical course has to be known. Calculation of the position error expressed in the *l-frame* is performed according to (1–4) (in this case the coordinates of the reference point are the ones of the *l-frame* origin). A disadvantage of this algorithm is neglecting the Earth's curvature in calculations (Fig. 4). Consequently, with increasing the distance from the *l-frame* origin, the position error in the D axis (δD) also increases (for the distance of 100 m – $\delta D \approx 7.8 \cdot 10^{-4}$ m, for the distance of 1000 m – $\delta D \approx 0.08$ m).

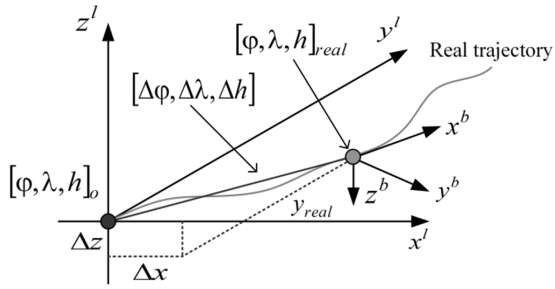

Fig. 3. The vector of position differences in algorithm II.

Metrol. Meas. Syst., Vol. 23 (2016), No. 3, pp. 383–391.

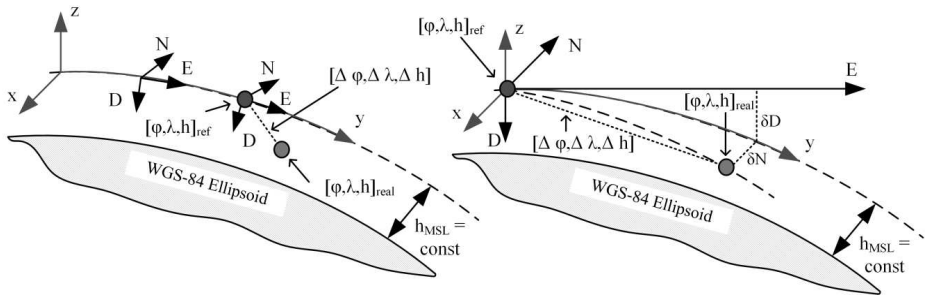

Fig. 4. The difference between algorithm I (left) and II (right) in interpretation of the Earth shape.

3. Results of field experiments

The practical tests of the first algorithm were carried out using a wheeled, land-based platform. The platform was moving along a rectangular-shaped trajectory (Fig. 5).

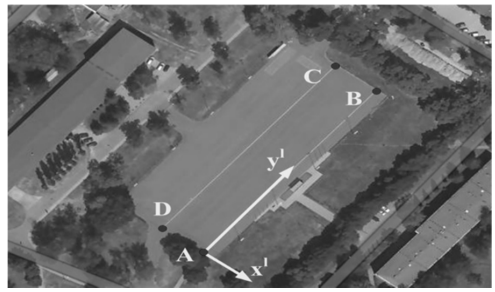

Fig. 5. The area of field tests (algorithm I).

The results of calculations of position deviations along the x^l and z^l axes, position and velocity along the y^l axis, are shown in Figs. 6–9. The assumed theoretical parameters of motion were: course $\Psi = 39\,°$, velocity along the y^l axis $v_{teor} = 1.5$ m/s, theoretical altitude $h_{teor} = 108$ m. Between points A and B, the movement took place along y^l axis, perpendicular to the x^l axis – thus a linear increase in the value of y position and close to zero value of x position were observed. The non-zero value of x position was a result of a small difference between the real and the theoretical course. For other sections of trajectory (BC, CD, DA) similar conclusions can be drawn. The aim of this test was to verify correctness of the proposed algorithm.

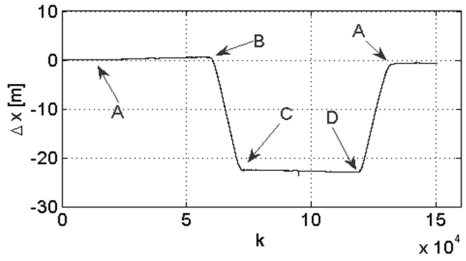

Fig. 6. The position error along the x^l axis.

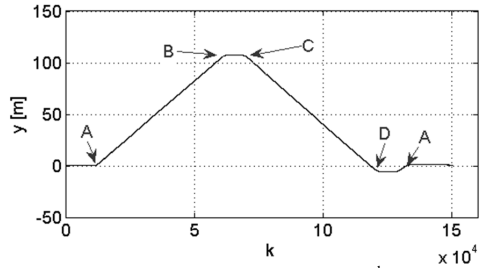

Fig. 7. The position along the y^l axis.

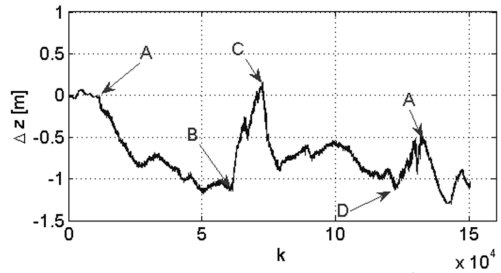

Fig. 8. The position error along the z^l axis.

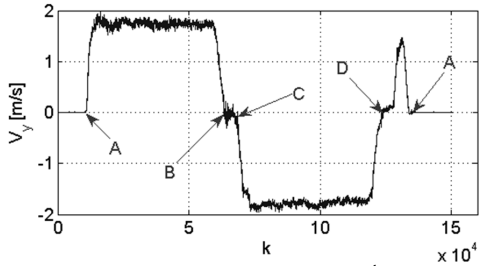

Fig. 9. The velocity along the y^l axis.

The practical tests of the second algorithm were performed using an UAV. A flight trajectory is shown in Fig. 10.

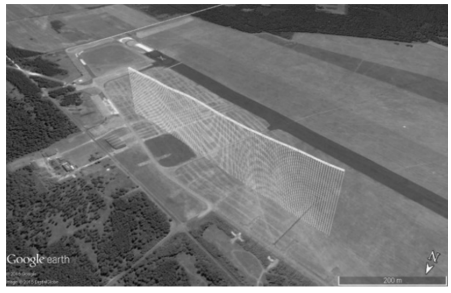

Fig. 10. The flight path.

The autopilot of UAV was supposed to control flight between two user-defined points, maintaining its straightness. The flight course was determined during post-processing, between the first (A), and the last (B) points of the recorded trajectory (Fig. 11).

Metrol. Meas. Syst., Vol. 23 (2016), No. 3, pp. 383–391.

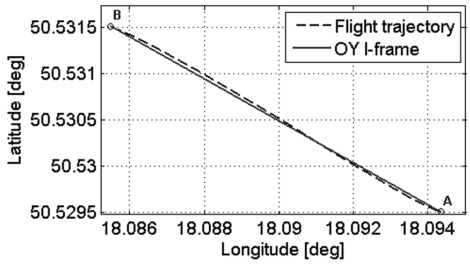

Fig. 11. The real and theoretical flight trajectories.

The results of navigation calculations are shown in Figs. 12–15.

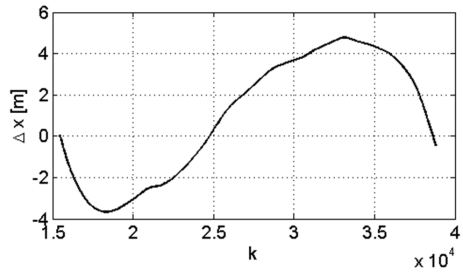

Fig. 12. The position error along the x^l axis.

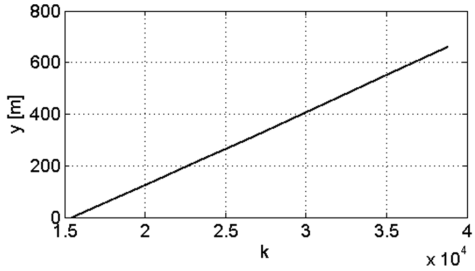

Fig. 13. The position measured along the y^l axis.

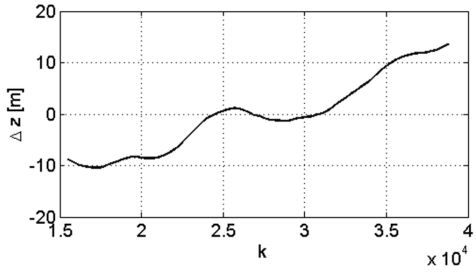

Fig. 14. The position error along the z^l axis.

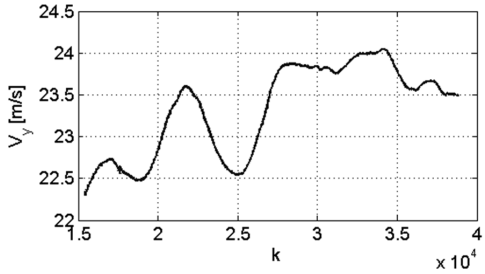

Fig. 15. The velocity measured along the y^l axis.

The measuring session chosen in the presented experiment lasted approximately 29 seconds but the time of aperture synthesis was limited to about 1 second. During this time, the UAV flew the distance of 24 m and the error resulting from the curvature of Earth was equal to only 0.005 mm. Consequently, in the proposed system, this error is irrelevant, especially when compared to the errors of navigation system. For this reason the Earth's curvature error can be neglected. It should be mentioned that determination of the course on the basis of the measurement data is not an obvious task, taking into consideration that the flight path may significantly differ from a straight line. For example, in the case of a measurement session in which the trajectory is composed of a straight line and a turn, the course of flight should be determined on an arbitrarily chosen straight section of the trajectory. Therefore, the navigation corrections depend not only on deviations from the assumed trajectory, but also on the correctness of choosing the theoretical course.

4. Conclusion

The paper presents two algorithms for determining navigation corrections used in the SAR image processing. The aim of these algorithms is to determine the set of navigational parameters for each SAR measurement: position errors along the x^l and z^l axes, position and velocity along the y^l axis. The navigational computations are performed using data obtained from the inertial sensors and the GNSS receiver with RTK option (RTK enables to obtain the 2.5 cm position accuracy). The proposed algorithms differ in interpretation of the Earth's shape. Neglecting the Earth's curvature is acceptable in systems in which UAV moves along relatively short distances during aperture synthesis. Apart from the issue of curvature, the second algorithm does not use the theoretical velocity of flight, which is a significant simplification comparing to the first algorithm. Taking into account these conclusions, the second algorithm was implemented in NDPM. The presented versions of algorithms calculate only discrepancy between the assumed and the measured location of the UAV COG. Further improvements could be obtained by augmentation of the navigational computations with a lever arm correction between an antenna phase center and the UAV COG.

Acknowledgement

This project was supported by the National Centre for Research and Development, Poland, within the frame of Applied Research Programme under Research Project PBS/B3/15/2012.

References

[1] Mengdao, X., Xiuwei, J., Renbiao, W., Feng, Z., Zheng, B. (2009). Motion Compensation for UAV SAR Based on Raw Radar Data. *IEEE Transactions an Geoscience and Remote Sensing*, 8, 2870–2883.

Metrol. Meas. Syst., Vol. 23 (2016), No. 3, pp. 383–391.

[2] Zaugg, E.C., Long, D.G. (2008). Theory and application of motion compensation for LFM-CW SAR. *IEEE Transactions an Geoscience and Remote Sensing*, 10, 2990–2998.

[3] Samczynski, P., Malanowski, M., Gromek, D., Gromek, A., Kulpa, K., Krzonkalla, J., Mordzonek, M., Nowakowski, M. (2014). Effective SAR image creation using low cost INS/GPS. *15th International Radar Symposium*, Gdańsk, 174–177.

[4] Fornaro, G. (1999). Trajectory deviations in Airborne SAR: Analysis and Compensation. *IEEE Transactions on Aerospace and Electronics Systems*, 3, 997–1009.

[5] Bekir, E. (2007). *Introduction to modern navigation systems*. World Scientific Publishing Co. Pre. Ltd., Singapore, 75–84.

[6] De Angelis, A., Nilsson, J.O., Skog, I., Handel, P., Carbore, P., (2010). Indoor Positioning by Ultrawide Band Radio Aided Inertial Navigation. *Metrol. Meas. Syst.*, 17(3), 447–460.

[7] Brown, R.G., Hwang, P.Y.C., (1997). *Introduction to random signals and applied Kalman filtering*. John Wiley & Sons, UK, 141–151.

[8] Konatowski, S. (2010). The development of nonlinear filtering algorithms. *Przeglad Elektrotechniczny*, 9, 272–277.

[9] Śmieszek, M., Dobrzańska, M. (2015). Application of Kalman Filter in Navigation Process of Automated Guided Vehicles. *Metrol. Meas. Syst.*, 22(3), 443–454.

[10] Li, X., Xie, Y., Bi, D., Ao, Y. (2013). Kalman Filter Based Method for Fault Diagnostics of Analog Circuits. *Metrol. Meas. Syst.*, 20(2), 307–322.

[11] Titterton, D.H., Weston, J.L. (2004). *Strapdown Inertial Navigation Technology*. Institution of Electrical Engineers, UK, 17–57.